Effect of Pressure on Argon Dielectric Barrier Discharge

A. Bouchikhi*

University of Saïda, Faculty of Technology, Department of Electrical Engineering, Saïda 20000, Algeria

Received: 17.02.2022 & Accepted: 27.04.2022

Doi: 10.12693/APhysPolA.142.249 *e-mail: bouchikhiabdelaziz1@yahoo.fr

In this work, we study the argon dielectric barrier discharge with metastable atom density on a capacitive coupled radio frequency at a pressure of 1–6 Torr. The transport parameter of argon depends on the mean electron energy, and its range is about 0.04–42 eV. The one-dimensional fluid model and the drift-diffusion theory were utilised to describe the argon dielectric barrier discharge. The effect of pressure on the properties of argon dielectric barrier discharge is presented on the cycle-averaged diet, especially on particle density, electric potential, and metastable atom density. Consequently, the values of these quantities increase with increasing pressure. In addition, the surface charge concentration and the gap voltage also increase.

topics: argon RF discharge, dielectric barrier, moments of Boltzmann's equation, Poisson's equation

1. Introduction

Glow discharge plasma [1–8] produced by a powered direct current (DC) or radio frequency (RF) source has a wide range of applications in industrial technologies and medical therapy. These include improved discharge by substance vapour deposition, surface adaptation with different materials, and plasma etching. Furthermore, the capacitive geometry can enhance these technologies [9]. Plasma etching is a progression technique for controlling the discharge by means of a dielectric barrier [10–13] at low and high pressure gases. In the medical domain, we can find dermatology treatments using coherent and incoherent ultraviolet (UV) and vacuum ultraviolet (VUV) radiation from a glow source.

Apart from the experimental tools [14], the mathematical model is the best technique for describing and optimizing the discharge behaviour, mainly at the sides of the electrodes and in the bulk plasma. Samir et al. [15] investigated the effect of gas pressure on the capacitive coupled radio frequency argon gas discharge. Thus, the electric potential increases and the electron temperature decreases with increasing gas pressure. Liu et al. [16] studied the effect of the secondary electron emission coefficient (SEEC) on the capacitive coupled radio frequency (CCRF) argon glow discharge. Authors demonstrated that increasing SEEC consequently changes many parameters, such as net power absorption, electron power dissipation and thermal conductive term. Becker et al. [17] presented a comparative study between argon and helium CCRF discharge using an advanced fluid model and particle-in-cell/Monte Carlo code.

Barjasteh and Eslami [18] described the discharge behaviour in dielectric barrier discharges in a low-pressure 90%Ar–10%Cl_2 gas mixture. It has been shown that the electronegativity properties and the radiation process grow when voltage amplitude increases. However, when the frequency increases, the electronegativity properties decrease. Barjasteh et al. [19] studied the effect of voltage parameters on dielectric barrier discharge (DBDs) at low-pressure argon gas. They have shown that an increase in the applied voltage and frequency causes a considerable increase in the radiation process and current discharge.

In this manuscript, we provide a detailed description of the behaviour of argon glow discharge operating in CCRF and controlled by a dielectric barrier in the presence of a metastable atom density. Moreover, the effect of gas pressure on plasma characteristics was investigated.

2. Physical model and boundary condition

The description of our discharge, depicted in Fig. 1, is modelled in a one-dimensional geometry. This assumption is due to the fact that the side of the electrode is larger than the inter-electrodes spacing. The fluid model is then used to account for the RF argon plasma. This is valid when we utilize

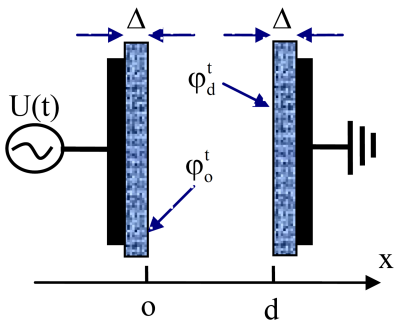

Fig. 1. Discharge configuration; φ_x^t is the electric potential at the dielectric side.

the frequency set to 13.56 MHz, and the argon gas pressure is supplemented to 1–6 Torr. Therefore, the RF driving frequency is less than the momentum transfer collision frequency.

For an ample explanation of low-pressure argon plasma, atomic and argon ions and excited atomic ions were taken into account. Therefore, the kinetic scheme of the processes includes five electron collision reactions, named elastic collision, ionisation, excitation, de-excitation, and stepwise ionisation. These processes are related to rate coefficients, which are dependent on the mean electron. The coefficients are labelled as follows: P_{ec}, k_{io}, k_{ex}, K_{dex}, and K_{io}^m, respectively.

In addition, the chemo-ionisation (K_{ci}) [20] and the radiation processes (τ_m) [21] are considered. Table I abstracts these reactions and their references [20–25]. The processes k_{io}, k_{ex} and K_{dex} are calculated using BOLSIG+ software [22, 23], and the process K_{io}^m is determined according to the expression given by Vriens and Smeets [24]. The model [6, 7] is then given by relations

$$\frac{\partial n_e}{\partial t} + \frac{\partial \Gamma_e}{\partial x} = S_e, \tag{1}$$

$$\frac{\partial n_+}{\partial t} + \frac{\partial \Gamma_+}{\partial x} = S_+, \tag{2}$$

$$\frac{\partial n_m}{\partial t} + \frac{\partial \Gamma_m}{\partial x} = S_m, \tag{3}$$

$$\frac{\partial (\varepsilon_e n_e)}{\partial t} + \frac{\partial \Gamma_{e\varepsilon}}{\partial x} = S_{e\varepsilon}, \tag{4}$$

$$S_e = S_+ = n_e n_g K_{io} + n_e n_m K_{io}^m + n_m n_m K_{ci}, \tag{5}$$

$$S_m = n_e n_g K_{ex} - n_e n_m K_{dex} - n_e n_m K_{io}^m - 2 n_m n_m K_{ci} - \frac{n_m}{\tau_m}, \tag{6}$$

$$\Gamma_e = -n_e \mu_e E - \frac{\partial (D_e n_e)}{\partial x}, \tag{7}$$

$$\Gamma_+ = n_+ \mu_+ E - \frac{\partial (D_+ n_+)}{\partial x}, \tag{8}$$

$$\Gamma_m = -D_m \frac{\partial n_m}{\partial x}, \tag{9}$$

$$\Gamma_{e\varepsilon} = -n_e \mu_{e\varepsilon} E - \frac{\partial (D_{e\varepsilon} n_e)}{\partial x}, \tag{10}$$

$$S_{e\varepsilon} = -e\Gamma_e E + \varepsilon_m n_e n_m K_{dex} + \varepsilon_{ci} n_m n_m K_{ci} - n_e P_{ec} - \varepsilon_m n_e n_g K_{ex} - \varepsilon_{io} n_e n_g K_{io} - \left(\varepsilon_{io} - \varepsilon_m\right) n_e n_m K_{io}^m, \tag{11}$$

$$\frac{\partial^2 \varphi}{\partial x^2} = -\frac{e_o}{\varepsilon_o}\left(n_+ - n_e\right). \tag{12}$$

Synonyms of the different notations utilized in the above equations are mentioned in Table II.

2.1. Boundary conditions

In this subsection, we will present the initial and boundary conditions. There are many boundary conditions, and they are established in different written expressions, as quoted by Samir et al. [15]

TABLE I

Kinetic scheme of processes and their rate coefficients with units ([eV/s], [cm^3/s], [s], and [cm^6/s]).

Processes	Rates coefficients	Refs.
$Ar + e^- \rightarrow Ar + e^-$	P_{ec} [eV s^{-1}]	[25]
$Ar + e^- \rightarrow Ar^+ + 2e^-$	k_{io} [cm^3 s^{-1}]	[22, 23]
$Ar + e^- \rightarrow Ar_m^* + e^-$	k_{ex} [cm^3 s^{-1}]	[22, 23]
$Ar_m^* + e^- \rightarrow Ar + e^-$	K_{dex} [cm^3 s^{-1}]	[22, 23]
$Ar_m^* + Ar_m^* \rightarrow Ar^+ + e^- + Ar$	K_{ci} [cm^6 s^{-1}]	[20]
$Ar_m^* \rightarrow Ar + h\nu$	τ_m=10^{-7} [s]	[21]
$e^- + Ar_m^* \rightarrow Ar^+ + 2e^-$	K_{io}^m [cm^3 s^{-1}]	[24]

TABLE II

Description of the different notations utilized in our model. The subscript (s) can stand for: electron (e), positive ions (+), metastable atoms (m), electron energy (ε_e).

Notations	Description
n_s	particle density of species (s)
ε_e	mean electron energy
Γ_s	particle flux of species (s)
Φ	electrostatic potential
n_g	neutral gas density
S_s	source term of species (s)
D_s	diffusion coefficient of species (s)
E	electric field
ε_o	free space permittivity
e_o	elementary charge
μ_s	mobility of species (s)

TABLE III

Discharge configuration and argon physical characteristics applied in CCRF dielectric barrier discharge with E/n_g in [Td].

Symbol	Definition	Value	Refs.
d	electrode distance [cm]	1	–
$T_{\rm gas}$	gas temperature [K]	300	–
p	pressure [Torr]	1, 3 and 6	–
U_a	voltage amplitude [V]	250	–
f	frequency [MHz]	13.56	–
$n_g\mu_e$	electron mobility [$\mathrm{V^{-1}cm^{-1}s^{-1}}$]	BOLSIG+	[22, 23]
$n_g D_e$	electron diffusivity [$\mathrm{cm^{-1}s^{-1}}$]	BOLSIG+	[22, 23]
W_+	ion drift velocity [m/s]	$\frac{4E/n_g}{\sqrt[3]{1+\left(0.007E/n_g\right)^{\frac{3}{2}}}}$	[28]
D_+	ion diffusivity [$\mathrm{m^{-1}s^{-1}}$]	$\frac{\mu_+ k_{\rm B} T_{\rm gas}}{e_o}$	–
K_s	electron recombination coefficient [cm/s]	1.19×10^{7}	[16]
γ	electron emission coefficient	0.06	–

and Liu et al. [16]. The boundary conditions in the presence of the dielectrics can be arranged accordingly:

- The ion flux and electron temperature at each electrodes are $\Gamma_+ = n_+\mu_+E$ and T_e=0.5, and at ground electrode ($x = d$) as Γ_e=$-n_eK_s$-$\gamma\Gamma_+$.
- The discharge reactor is powered at ($x = 0$) by a sinusoidal voltage $U(t) = U_a \sin(2\pi ft)$, and at ground electrode ($x = d$) by $U(t) = 0$.
- Initial densities are chosen in Gaussian form, i.e., n_e=n_+=10^7+$10^9\left(1-\frac{x}{d}\right)^2\left(\frac{x}{d}\right)^2$ [$\mathrm{cm^{-3}}$].

In order to discover the accumulation of surface charges on dielectrics, the Gauss law [10] is applied

$$\varepsilon_r\varepsilon_o\, E_{\rm diel}(x,t)\,\nu - \varepsilon_o\, E(x,t)\,\nu = \sigma_s(x,t), \qquad (13)$$

where $E_{\rm diel}(x,t)$ is the electric field inside the dielectric and ε_r is its relative permittivity, and $E(x,t)$ is the electric field related to the gas discharge.

To compute the electric potential on dielectrics (φ_0^t and φ_d^t), we have employed (13). The temporal evolution of the surface charge density ($\sigma_s(x,t)$) begins from the breakthrough of particle currents by dielectrics and is expressed by Becker et al. [14] as

$$\frac{\partial\sigma_s(x,t)}{\partial t} = e_o\sum_j \Gamma_j(x,t)\,\nu. \qquad (14)$$

The set of partial differential equations is discretized using the finite difference method. More clearly, the transport particle and energy equations have been discretized according to an exponential scheme [26, 27]. Poisson's equation has been spatially discretized by means of the central difference technique. Both steps in the time and space grids are taken as uniform and constant. The number of grid points in space was equal to 250, and the time period was equal to 4×10^3. The argon transport parameters are reported in Table III.

3. Results and discussion

Figure 2 shows the profiles of the electric potential as a function of the electrode distance d for different pressure values during the 2000th cycle CCRF argon dielectric barrier discharge, and these profiles are given in the cycle-averaged diet. Note that the electrical potential is greater when the gas pressure is 6 Torr than when the gas pressure is 3 Torr. And the electric potential of the latter is greater than that of the gas pressure of 1 Torr. We knew that the augmentation of the gas pressure extends the plasma region, and then the electric potential extends too, i.e., the width occupied by the plasma region of the electric potential increases with increasing the gas pressure. The behaviour of the electric potential is characterized by two sheath thicknesses between which the bulk plasma region is located. This behaviour is again characterized by the maximum and minimum values of the potential. We can then know the landing potential as the difference between the maximum and minimum values of the electric potential. Consequently, the landing potential is equal to 122.47, 111.37, and 104.37 V when the pressure is 1, 3, and 6 Torr, respectively. We remark that the landing potential decreases with increasing pressure.

Figure 3 represents the metastable atom density as a function of d for different pressure values during the 2000th cycle CCRF argon dielectric barrier discharge. Figure 3 shows the cycle-averaged values. We remark that the typical metastable atom density has a symmetric form compared to the density profile shown in Fig. 3 in the middle of the inter-electrode spacing. Consequently, the metastable atom densities are characterised by two summits. We can see that the metastable atom density increases with increasing pressure. This is due to the augmentation of the gas density and, subsequently,

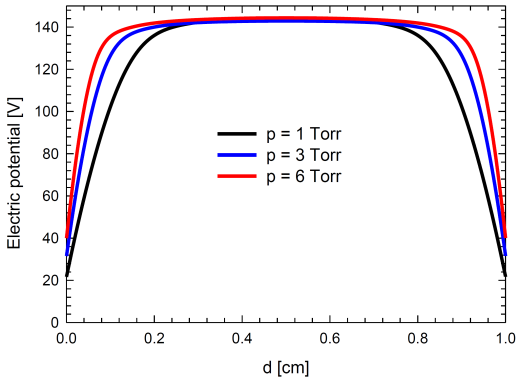

Fig. 2. Electric potential profiles as a function of electrode distance d for different pressure values in the 2000th cycle CCRF argon dielectric barrier discharge, and these profiles are provided in the cycle-averaged diet.

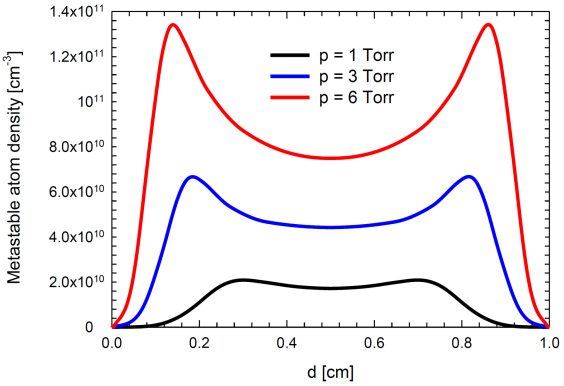

Fig. 3. Metastable atom density curves in the 2000th cycle CCRF argon dielectric barrier discharge as a function of d for different pressure values. These curves are cycle-averaged.

the augmentation of the excitation processes. Obviously, the maximum of the metastable atom density evolves from 2.09×10^{10} to 1.34×10^{11} cm^{-3} when the pressure evolves from 1 to 6 Torr.

Figure 4 outlines the electron temperature as a function of the electrode distance for different pressure values during the 2000th cycle CCRF argon dielectric barrier discharge, and these results are computed based on a cycle-averaged diet. As one can see, the electron temperature is characterized by two peaks between which the temperature is decreased. This distribution is caused by a higher gradient of potential at both electrodes. Then the strong electron fluxes are presented. Therefore, a heating phenomenon occurs at both electrodes, which seems to contrast with the cooling phenomenon created by the electron density and argon ground state and threshold ionisation or excitation. In the bulk plasma region, the cooling phenomenon is greater due to the presence of a higher electron density. We remark that the electron temperature decreases with increasing

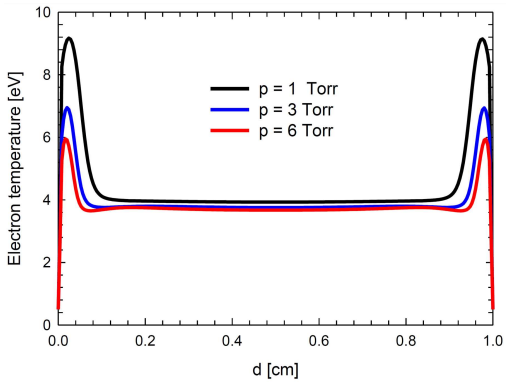

Fig. 4. Electron temperature outlines the dependence on the pressure in the 2000th cycle CCRF argon dielectric barrier discharge. These outlines are computed based on a cycle-averaged diet.

TABLE IV

Summary of the plasma density and the electric field as a function of pressure in 2000 cycle-averaged CCRF argon dielectric barrier discharge.

Pressure [Torr]	Plasma density [cm^{-3}]	Electric field [V/cm]
1	6.62×10^{9}	997.26
3	1.52×10^{10}	1451.83
6	2.56×10^{10}	1844.13

pressure. This is due to the diminution of the mean free path, which leads to diminishing the energy of the electron. As a result, electron temperatures diminish in both the sheath and in the bulk plasma.

Obviously, the electron temperature decreases from 9.17 to 5.95 eV at the sheath thickness and decreases from 3.93 to 3.67 eV in the bulk plasma region when the pressure increases from 1 to 6 Torr.

In order to show the discharge behaviour, we summarized the plasma density and electric field as a function of pressure in the 2000 cycle-averaged CCRF argon dielectric barrier discharge in Table IV. As one can see, plasma density increase with pressure from 6.62×10^{9} to 2.56×10^{10} cm^{-3}. This is due to the augmentation of chemical processes. These collision processes are ionisation, stepwise ionisation, and chemo-ionisation, which lead to an increase in the densities of particles. As a consequence, the electric field increases with pressure from 997.26 to 1844.13 V/cm.

In order to validate our numeric code, we have investigated our discharge without dielectrics and compared our results to those given by Park and Economou [29], Meyyappan and Govindan [30], Hwang et al. [31], Surendra and Vender [32], and Surendra et al. [33]. We obtained a reasonable agreement.

Figure 5 shows the effect of pressure on the gap voltages as a function of reduced periodic of CCRF argon dielectric barrier discharge during the 2000th

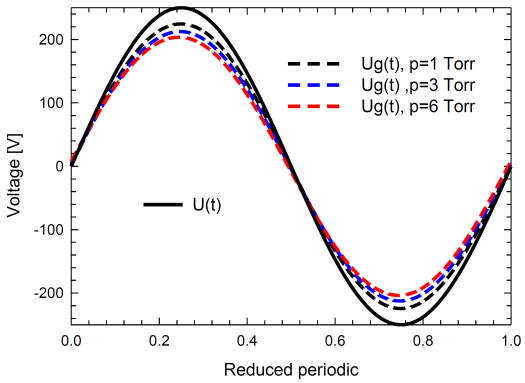

Fig. 5. Effect of pressure on the gap voltages as a function of the reduced periodic of CCRF argon dielectric barrier discharge during the 2000th cycle. Here, $U(t)$ is the applied voltage.

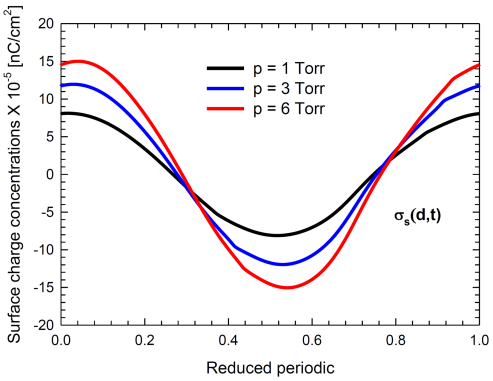

Fig. 6. Effect of pressure on the surface charge concentrations $\sigma_s(d,t)$ as a function of the reduced periodic of CCRF argon dielectric barrier discharge during the 2000th cycle.

cycle. To examine this effect, we plotted the applied voltage ($U(t)$). We defined the gap voltage as $U_g(t) = \varphi_0^t - \varphi_d^t$. Consequently, the gap voltage is lower than the applied voltage. It is worth noting that the resulting form of the gap voltage is sinusoidal. This is due to the source voltage, which has a sinusoidal form. The amplitude of the gap voltage is decreased to 224.41, 212.42, and 203.49 V when the gas pressure is 1, 3, and 6 Torr, respectively. As a result, the difference between the applied voltage and the gap voltage is about 25.59, 37.58, and 46.51 V. We remark that the voltage difference increases with increasing pressure.

Figure 6 shows the effect of pressure on the surface charge concentrations ($\sigma_s(d,t)$) as a function of the reduced periodic of CCRF argon dielectric barrier discharge during 2000th cycle. The morphology of $\sigma_s(d,t)$ strictly follows the structure of the gap voltage. The surface concentrations reflect the precipitation of the particle charged on the dielectrics, and this precipitation increases with time. As one can see, the surface concentration $\sigma_s(d,t)$ increases with increasing pressure. For

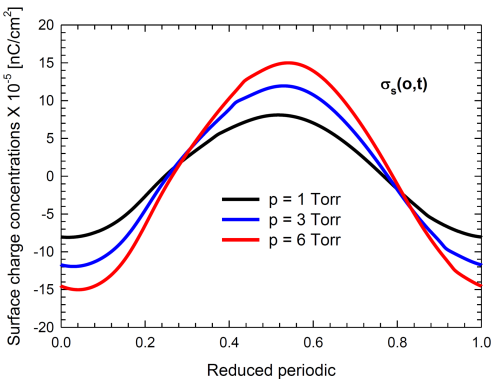

Fig. 7. Effect of pressure on the surface charge concentrations $\sigma_s(o,t)$ as a function of the reduced periodic of CCRF argon dielectric barrier discharge during the 2000th cycle.

example, the maximum evolves from 8.11×10^{-5} to 15.01×10^{-5} nC/cm^2 when the pressure changes from 1 to 6 Torr, which is due to the augmentation of the electric field at the electrodes.

Figure 7 shows the effect of pressure on the surface charge concentrations $\sigma_s(o,t)$ as a function of the reduced periodic of CCRF argon dielectric barrier discharge during 2000th cycle. As one can see, the morphology of $\sigma_s(o,t)$ has the same behaviour as $\sigma_s(d,t)$ and has a reversed polarity, i.e., the surface charge concentration $\sigma_s(d,t)$ has the maximum value, the surface charge concentrations $\sigma_s(o,t)$ has the minimal value, and vice versa. Also, this morphology is conserved in each period. The effect of pressure on $\sigma_s(o,t)$ is similar to the effect described for $\sigma_s(d,t)$, and the amplitude of $\sigma_s(o,t)$ evolves from 8.10×10^{-5} to 14.99×10^{-5} nC/cm^2 when the pressure evolves from 1 to 6 Torr. This result is due to the augmentation of the electric field at the electrodes.

Figure 8 shows the effect of pressure on the electron current during the 2000th cycle CCRF argon dielectric barrier discharge at the phase $wt = \pi$. We remark that the electron current is characterized by two sheath thicknesses located at both electrodes and the plasma region. As one can see, the effect of pressure is independent of both sheath thicknesses. However, in the plasma region, the electron current increases with increasing pressure due to the augmentation of the electron density being present. Moreover, we notice that the electron current is quasi-constant in the plasma region. The maximum of the electron current is 4.32, 6.3, and 7.78 mA/cm^2 when the pressure is equal to 1, 3, and 6 Torr, respectively.

Figure 9 shows the effect of pressure on the ion current during the 2000th cycle CCRF argon dielectric barrier discharge at the phase $wt = \pi$. We remark that the spatial distribution of the ion current is symmetric in the middle of the inter-electrode spacing d. This situation is due to the

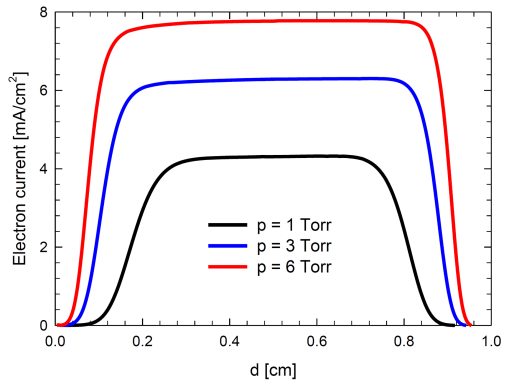

Fig. 8. Effect of pressure on the electron current during the 2000th cycle CCRF argon dielectric barrier discharge at the phase $wt = \pi$.

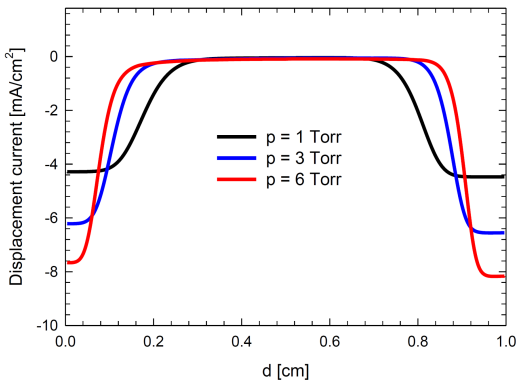

Fig. 10. Effect of pressure on the displacement current during the 2000th cycle CCRF argon dielectric barrier discharge at the phase $wt = \pi$.

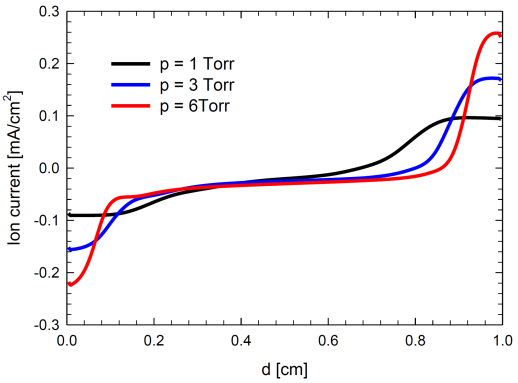

Fig. 9. Effect of pressure on the ion current during the 2000th cycle CCRF argon dielectric barrier discharge at the phase $wt = \pi$.

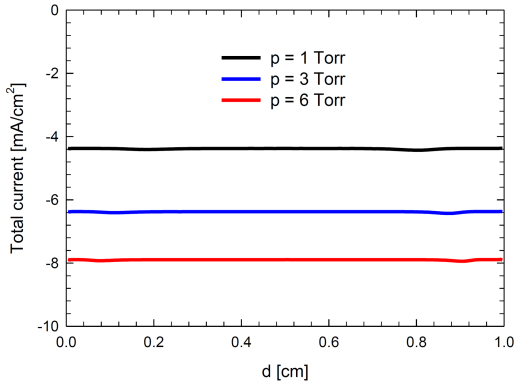

Fig. 11. Effect of pressure on the total current during the 2000th cycle CCRF argon dielectric barrier discharge at the phase $wt = \pi$.

impact of the electric field on the ion current. As one can see, the ion current increases as pressure increases due to the expansion of the plasma region. The maximum of the ion current evolves from 0.1 to 0.26 mA/cm^2 when the pressure evolves from 1 to 6 Torr.

Figure 10 shows the effect of pressure on the displacement current during the 2000th cycle CCRF argon dielectric barrier discharge at the phase $wt = \pi$. We remark that the spatial distribution of the displacement current is characterized by two sheath thicknesses located at both electrodes, and there is a plasma region between them. However, as one can observe, the behaviour of the displacement current is different from that of the electron current. On the one hand, the profile of the displacement current does not change regardless of the pressure. On the other hand, the displacement current value increases with increasing pressure. It is obvious that the maximum displacement current is 4.47, 6.55, and 8.17 mA/cm^2 when the pressure is equal to 1, 3, and 6 Torr, respectively. In the plasma region, the displacement current is null regardless of pressure.

Figure 11 shows the effect of pressure on the total current during the 2000th cycle CCRF argon dielectric barrier discharge at the phase $wt = \pi$. The total current represents the sum of the electron, ion, metastable atom, and displacement currents. Furthermore, the current of the metastable atom is negligible and, therefore, not shown. Hence, the fall in both the electron current and displacement currents fades away between them, and the total current is constant at inter-electrodes spacing. The total current at the phase $wt = \pi$ is -4.37, -6.37, and -7.89 mA/cm^2 when the pressure is equal to 1, 3, and 6 Torr, respectively.

4. Conclusion

Three moments of Boltzmann's equation (1)–(4) with Poisson's equation (12) are taken to describe capacitive coupled argon glow discharge, driven by radio frequency power at low pressure with dielectrics. In addition, the metastable atom density was reintroduced in the model. We have used the particle flux expression to describe the model because it can explain the electrons and ions kinetic

in both electrodes. Furthermore, Gauss's law explains the accumulation of a charged particle on dielectrics. The effect of the boundary conditions in the presence of dielectric is well defined by the spatial distribution of surface charge concentrations and the gap voltage over time. The effect of pressure on the discharge characteristic is presented within the cycle-averaged. The increase in pressure leads to the following results:

- particle densities, electrical field, and electrical potential increase;
- surface charge concentration and gap voltage increase;
- electron temperature decreases;
- current increases.

With an electrode spacing of 1 cm, a voltage amplitude of 250 V, a frequency of 13.56 MHz, a gas pressure of 3 Torr, and a SEEC of 0.06, the characteristic discharge causes that

- the maximum particle density is 1.52×10^{10} cm^{-3};
- the maximum electron temperature is 6.95 eV;
- the current at the phase $wt=\pi$ is -6.37 mA/cm^2;
- the electrode electric field is 1451.83 V/cm.

References

[1] T. Samir, Y. Liu, L.-L. Zhao, Y.-W. Zhou, *Chin. Phys. B* **26**, 115201 (2017).

[2] L.-L. Zhao, Y. Liu, T. Samir, *Chin. Phys. B* **26**, 125201 (2017).

[3] M. Meyyappan, J.P.L. Kreskovsky, *J. Appl. Phys.* **68**, 1506 (1990).

[4] B. Hechelef, A. Bouchikhi, *Acta Phys. Pol. A* **136**, 855 (2019).

[5] M.M. Becker, D. Loffhagen, *AIP Adv.* **3**, 012108 (2013).

[6] M.M. Becker, D. Loffhagen, W. Schmidt, *Comp. Phys. Com.* **180**, 1230 (2009).

[7] A. Bouchikhi, *Can. J. Phys.* **96**, 62 (2018).

[8] A. Bouchikhi, *IEEE Trans. Plasma Sci.* **9**, 4260 (2019).

[9] Y. Lin, R.A. Adomaitis, *J. Comp. Phys.* **171**, 731 (2001).

[10] D. Loffhagen, M.M. Becker, A.K. Czerny, J. Philipp, C. Klages, *Contrib. Plasma Phys.* **58**, 337 (2018).

[11] S. Ponduri, M.M. Becker, S. Welzel, M.C.M. van de Sanden, D. Loffhagen, R. Engeln, *J. Appl. Phys.* **119**, 093301 (2016).

[12] H. Höft, M. Kettlitz, M.M. Becker, T. Hoder, D. Loffhagen, R. Brandenburg, K.-D. Weltmann, *J. Phys. D: Appl. Phys.* **47**, 465206 (2014).

[13] E. Eslami, A. Barjasteh, N. Morshedian, *Plasma Phys. Rep.* **41**, 519 (2015).

[14] M.M. Becker, T. Hoder, R. Brandenburg, D. Loffhagen, *J. Phys. D: Appl. Phys.* **46**, 355203 (2013).

[15] T. Samir, Y. Liu, L.-L. Zhao, *IEEE Trans. Plasma Sci.* **46**, 1738 (2018).

[16] Q. Liu, Y. Liu, T. Samir, Z. Ma, *Phys. Plasmas* **21**, 083511, (2014).

[17] M.M. Becker, H. Kählert, A. Sun, M. Bonitz, D. Loffhagen, *Plasma Sources Sci. Technol.* **26**, 044001 (2017).

[18] A. Barjasteh, E. Eslami, *Plasma Chem. Plasma Process.* **38**, 261 (2018).

[19] A. Barjasteh, E. Eslami, N. Morshedian, *Phys. Plasmas* **22**, 073508 (2015).

[20] N.B. Kolokolov, A.A. Kudrjavtsev, A.B. Blagoev, *Phys. Scr.* **50**, 371 (1994).

[21] I. Rafatov, E.A. Bogdanov, A.A. Kudryavtsev, *Phys. Plasma* **19**, 093503 (2012).

[22] G.J.M. Hagelaar, L.C. Pitchford, *Plasma Sources Sci. Technol.* **14**, 722 (2005).

[23] Plasma Data Exchange Project.

[24] L. Vriens, A.H.M. Smeets, *Phys. Rev. A* **22**, 940 (1980).

[25] W. Van Gaens, A. Bogaerts, *J. Phys. D Appl. Phys.* **47**, 079502 (2014).

[26] D.L. Scharfetter, H.K. Gummel, *IEEE Trans. Elec. Dev.* **16**, 64 (1969).

[27] A. Bouchikhi, *Indian J. Phys.* **94**, 353 (2020).

[28] A.V. Phelps, Z.Lj. Petrović, *Plasma Sources Sci. Technol.* **8**, R21 (1999).

[29] S.K. Park, D.J. Economou, *J. Appl. Phys.* **68**, 4888 (1990).

[30] M. Meyyappan, T.R. Govindan, *J. Appl. Phys.* **74**, 2250 (1993).

[31] S.W. Hwang, H.-J. Lee, H.J. Lee, *Plasma Sources. Sci. Technol.* **23**, 065040 (2014).

[32] M. Surendra, D. Vender, *Appl. Phys. Lett.* **65**, 153 (1994).

[33] M. Surendra, D. Graves, L.S. Plano, *J. Appl. Phys.* **71**, 5189 (1992).